High-angle, not low-angle, normal faults dominate early rift extension in the Corinth Rift

Rebecca E. Bell[1], Guillaume Duclaux[2*], Casey W. Nixon[2], Robert L. Gawthorpe[2], and Lisa C. McNeill[3]

[1]*Basins Research Group, Imperial College London, Prince Consort Road, South Kensington, London SW7 2BP, UK*

[2]*Department of Earth Science, University of Bergen, P.O. Box 7803, N-5020 Bergen, Norway*

[3]*Ocean and Earth Science, National Oceanography Centre Southampton, University of Southampton, European Way, Southampton SO14 3ZH, UK*

* *Now at Université Côte d'Azur, CNRS, OCA, IRD, Géoazur, 06560 Valbonne, France*

ABSTRACT

Low-angle normal faults (LANFs) accommodate extension during late-stage rifting and breakup, but what is more difficult to explain is the existence of LANFs in less stretched, early-stage continental rifts. A critical example is the <5 Myr old Corinth Rift, central Greece where microseismicity, the geometry of exposed fault planes and deep seismically imaged faults have been used to argue for the presence of <30° dipping normal faults. However, new and reinterpreted data calls into question whether LANFs have been influential in controlling the observed rift geometry, which involves i) exposed steep fault planes, ii) significant uplift of the southern rift margin, iii) 10s – 100s kyr time-averaged uplift to subsidence ratios across south coast faults of 1:1–1:2, and iv) north margin subsidence. We test whether slip on a mature LANF can reproduce the long-term (10s kyr) geometry and morphology of the Corinth Rift using a finite-element method, to model the uplift and subsidence fields associated with proposed fault geometries. Models involving LANFs at depth produce very minor coseismic uplift of the south margin and post-seismic relaxation results in net

subsidence. In contrast, models involving steep planar faults to the brittle-ductile transition produce displacement fields involving an uplifted south margin with uplift to subsidence ratios of ~1:2-3, compatible with geological observations. We therefore propose that LANFs cannot have controlled the geometry of the Corinth Rift over 10s kyr timescales. We suggest that although LANFs may become important in the transition to breakup, in areas that have undergone mild stretching, do not have significant magmatic activity, and do not have optimally orientated pre-existing low-angle structures, high-angle faulting will be the dominant strain accommodation mechanism in the upper crust during early rifting.

INTRODUCTION

Both high- and low-angle normal faults (dipping $<30^{o}$) have been proposed to accommodate strain at some early-stage continental rifts, including the Basin and Range, central Apennines, Aegean/Western Turkey and the Corinth Rift, Greece. Low angle normal faults (LANFs) present a paradox in structural geology as Andersonian theory would suggest that slip on LANFs is mechanically unfavorable (e.g. Sibson 1985). These continental rifts are therefore crucial case studies for assessing when in the rifting process, and under what conditions, LANFs become important in accommodating strain. In the Basin and Range an association between detachments (faults dipping $<15^{o}$) and magmatic activity has been reported, suggesting that igneous midcrustal inflation may rotate the stress field such that LANFs are favorable (Parsons and Thompson, 1993). Low-angle faults have been observed in Turkey, however these may have rotated from steeper angles to their current 0–20° dip angles (Gessner et al., 2001), rather than LANFs being a first-order extension mechanism. Low-angle normal faults have also been observed in the central Apennines where their origin has been linked to subduction roll-back (Collettini et al., 2006) or collapse of an over-thickened accretionary wedge, whereby thrust faults are reactivated as LANFs (Ghisetti and

Vezzani, 1999). These studies suggest that LANFs are only present in early-stage continental rifts under rather specific conditions.

A key example is the 3 – 30 km wide Corinth Rift, Greece, which at <5 Myr old and with a stretching factor of <1.4 (Bell et al. 2011) provides a snap-shot of the very early stages of continental rifting (Fig. 1a). The western part of the rift has long been used as an example of a setting where low-angle normal faulting plays a key role in strain accommodation (e.g., Jolivet et al., 2010; Sorel, 2000) and is commonly referred to by studies reviewing LANF mechanisms (e.g., Lecomte et al., 2012). The Corinth Rift is amagmatic and like the central Apennines it occurs within cold, orogenically thickened crust, however, the Corinth Rift runs orthogonal, not parallel, to the Hellenide orogeny. If early-stage continental extension at Corinth is really controlled by LANFs it would suggest that they may be a primary strain-accommodation mechanism in the earliest stages of continental rifting.

If a mature, seismically active LANF or detachment does exist beneath the western Corinth Rift, slip on such a structure must be able to account for the long-term (10s – 100s kyr) geometry and pattern of vertical displacement across the rift, which is well constrained from seismic reflection imaging and geomorphology data. The southern margin is uplifting with late Quaternary uplift rates of 0.8–2.0 mm/yr determined from uplifted marine terraces and wave-cut notches (e.g., Armijo et al., 1996; Palyvos et al., 2008). Long-term uplift to subsidence ratios across the largest faults bordering the southern margin are estimated at 1:1.2 – 1:2.2, measured from the elevation of features of comparable age in the footwall and hanging wall (McNeill et al., 2005; McNeill et al., 2007). In contrast, the northern margin appears to be dominated by subsidence (Bell et al., 2009; Elias et al. 2009). GPS data have been collected in the Corinth Rift, however Bell et al. (2011) show that GPS extension rate patterns are incompatible with the long-term rift geometry and cannot have persisted over a 100s kyr timescale.

In this study we perform new finite-element displacement modeling to investigate if LANFs are capable of reproducing the observed patterns of vertical displacement across the rift to definitively address the question "is Corinth an example of a rift that is dominated by low-angle normal faulting?" If the answer to this question is no, the elimination of this example would call into question the significance of LANFs during early stage rifting.

LOW- VERSUS HIGH-ANGLE DEEP FAULT GEOMETRY MODELS IN THE CORINTH RIFT

The shallow geometry of Corinth Rift active faults is known from exposed fault scarps onshore, with reported fault dips of 46–60° (e.g., Ford et al., 2013). Seismic reflection interpretations from different authors agree that the dip angle of offshore faults down to ~3 km ranges from 35 to 60° (e.g., Nixon et al., 2016; Taylor et al., 2011). However, controversy remains as to the geometry of faults deeper than 3 km as these have never been directly imaged. Two classes of deep fault geometry model have emerged:

Model 1–Low-angle (<30°) Active Faults at Depths >3 km

Rigo et al. (1996) proposed that microseismicity lies on a plane dipping 10–25° to the north at a depth of ~6–9 km below the south coast of the Gulf of Corinth (Fig. 1b). They interpreted this band of active seismicity as a low-angle detachment onto which steep faults observed at the surface sole into at depth. Syn-rift sediment depocenters in the northwestern Peloponnese have shifted north through time and although most of the faults in this area are moderate to steeply dipping (40–50°), the most southern and oldest fault is low angle (25°). Sorel (2000) proposed that this structure is a detachment extending northwards beneath observed steep faults in the western part of the rift (Fig. 1b). Sachpazi et al. (2003) and Taylor et al. (2011) interpreted from deep seismic reflection data a low-angle structure at a similar depth to Sorel's (2000) proposed detachment in the western rift (Fig. 1b and DR1). Some focal mechanisms determined for large (M6) earthquakes that have occurred in the

western rift may support relatively low-angle faulting, however, these are subject to the nodal plane that is selected as the active fault (Bernard et al. 1997).

Although Rigo et al. (1996) and Sorel (2000) are commonly cited together as studies in support of a low-angle detachment, the Sorel (2000) – Taylor et al. (2011) LANF is 3 km beneath the south coast of the Gulf, whereas the zone of microsesimicity is at 6–9 km depth (Fig. 1b).

Model 2–Moderate to High-angle Faults (35–60°) to Depths >3 km

Although there is debate in the western Corinth rift, focal mechanisms of large earthquakes in the eastern rift occurred on faults dipping at 40–50° (Jackson et al., 1982). Lambotte et al. (2014) resolve the western Corinth Rift seismicity pattern further, and note that in some locations the microseismicity cloud appears to dip 10–20° to the north, yet in others it is sub-horizontal or chaotic (Fig. 1b). They also observed seismicity beneath the clustered microseismicity cloud, which they suggest is the continuation of high-angle faults imaged at shallower depth and supports a high-angle fault model rather than an active detachment. Nixon et al. (2016) reinterpreted the deep seismic reflection data and suggest that N-dipping south margin faults remain moderate to steep (35–60°) below depths of 3 km (Figs 1b and DR1). Further evidence for high-angle faulting comes from McNeill et al. (2005), Bell et al. (2011) and Ford et al. (2013) who calculated total extension across the rift by summing fault heaves assuming a planar fault geometry. In the western Corinth Rift the amount of extension required for the observed basement subsidence and crustal thinning is in line with summed heaves across higher angle faults.

MODELING THE VERTICAL DISPLACEMENT FIELD

We use *PyLith*, a finite-element quasi-static formulation (Aagaard et al., 2013), to model the deformation associated with imposed fault slip in a simple layered continental crust and we solve the two-dimensional (2-D) surface uplift and subsidence fields for the two

contrasting fault geometry models. *PyLith* allows the coseismic displacement field associated with a particular magnitude of slip on a fault to be calculated and also the deformation associated with post-seismic relaxation to be recovered. Assuming linear rheologies, addition of these displacement fields is representative of the vertical deformation pattern caused by multiple seismic cycles over a 10s kyr timescale.

Our 2-D model includes a 10 km thick elastic upper crust overlying a 30 km thick viscoelastic lower crust layer, with a Newtonian rheology with constant viscosity of 10^{19} Pas, consistent with previously published models for the region (Fig. 2; Sachpazi et al. 2007; King, 1998). The Maxwell time for the viscoelastic material is 10 years and full relaxation of the model is achieved after ~30 k.y. (Fig. DR2). The model is 1000 km wide with free slip boundary conditions on the model sides and base, and a top free surface. We only consider deformation patterns in the central 100 km of the model to avoid boundary effects (Fig. 2). We impose a total of 200 m of normal slip along a prescribed fault (simulating the result of 30 kyr of earthquakes with a recurrence interval of 150 years and a displacement of 1 m) and let the system relax. We present our vertical deformation results normalized to show the amount of uplift and subsidence produced per meter of displacement on the fault and compare them to first-order observations of Corinth Rift vertical deformation. We also calculate the normalized horizontal deformation (extension produced per meter of fault displacement) between points 10 km on either side of the fault, to test how the magnitude of extension varies on high- versus low-angle faults (Fig. D3). We note that varying elastic and viscous layer thickness within realistic limits does not change the conclusions presented in this manuscript (Figs. DR4, DR5 and DR6). Changing the linear viscosity only changes the timescale of relaxation, not the final uplift to subsidence pattern.

To cover the full range of deep fault geometries proposed in the literature we test two classes of fault model. Model 1 involves a LANF at depth and two different scenarios are

tested: Model 1a) a planar fault with dip of 45° soles into a 15° N-dipping detachment at a depth of 7 km below the south coast (cf. Rigo et al., 1996); and Model 1b) a 45° fault, which changes to a dip angle of 20° at a depth of 3 km and extends to a brittle-ductile transition at 10 km depth (cf. Sorel, 2000; Taylor et al., 2011). Model 2 involves planar faults which dip at 45° (Model 2a) or 60° (Model 2b) to the brittle-ductile transition at a depth of 10 km (after Nixon et al., 2016).

Model 1

The coseismic vertical displacement field associated with moderately high-angle faults (45°) soling into a detachment at a depth of 7 km (Model 1a) and 3 km (Model 1b), generates a minor amount of coseismic uplift of the southern margin (< 0.01 m for every 1 m of slip), but an order of magnitude more uplift of the northern margin 20-25 km north of the surface trace of the fault (0.1 m for every 1 m of slip) (Figs. 3a, b). The coseismic uplift of the north margin occurs above where the low-angle fault tips-out, as is also observed in simple dislocation models for low-angle normal faulting (e.g. Resor 2008). The horizontal displacement between points 10 km either side of the fault associated with the coseismic response is 0.6-0.65 m of extension per m of slip on the fault for Models 1a and Model 1b (Fig. DR3). After 30 k.y. of post-seismic relaxation the overall vertical displacement profile changes considerably (Fig. 3a, b). The deformation across the rift associated with Models 1a and 1b involves overall subsidence of both the southern and northern margins (Fig. 3a, b). This contrasts markedly with the observed uplift (0.8 - 2 mm/yr) of the southern Gulf of Corinth coastline averaged over a 10s-100s kyr timescale.

Model 2

For both 45° and 60° normal faults (Models 2a and 2b) the model predicts considerable coseismic uplift of the southern margin (0.12 m and 0.22 m for every 1 m of slip for 45° and 60° faults, respectively) and subsidence of the northern margin (Fig. 3c, d). The

horizontal displacement between points 10 km either side of the fault associated with the coseismic response is 0.5 m of extension per m of slip for Model 2a and 0.3 m of extension per m of slip for Model 2b (Fig. DR3). After post-seismic relaxation the southern margin remains uplifted and the northern margin subsides. Uplift to subsidence ratios across south coast faults are 1:3.1 and 1:2.2 for 45 and 60° faults, respectively.

DISCUSSION AND CONCLUSIONS

Deformation associated with LANFs modelled over a 10s kyr timescale produces subsidence of the southern margin of the Corinth Rift, incompatible with the widespread indicators of uplift along the south coast (Fig. 3a, b). We suggest that the enhanced post-seismic subsidence is due to viscous flow in the lower crust balancing the gradient of gravitational potential energy generated by slip on the fault. In contrast, models involving moderate to steep faults to depths of 10 km predict uplift of the south margin and uplift to subsidence ratios of 1:3.1 and 1:2.2 for 45° to 60° faults, respectively, within the range of estimates from geological observations (Fig. 3c, d) (McNeill et al., 2005; McNeill et al., 2007). Crustal thickness in the Eratini-Aigion area is ~33-40 km (Sachpazi, et al. 2007); we note that reducing the crustal thickness of our model from 40 km to 30 km results in uplift:subsidence ratios of 1:2.3 and 1:1 for Models 2a and 2b respectively, providing an even better match to the geologically constrained ratios (Fig. DR6). Our models show that LANFs result in 2.2 times more coseismic extension than planar 60^{o} dipping faults for the same amount of normal slip (Fig. D5). These findings together with the fact that high-angle planar faults can account for the amount of total extension across the rift (Bell et al. 2011, Ford et al. 2013), lead us to conclude that high-angle normal faulting is the dominant mechanism of strain accommodation in the Corinth Rift. We support the conclusion of Lambotte et al. (2014) that if a LANF does exist in the western Corinth Rift it is incipient.

The elimination of Corinth as an example of a rift that deforms predominantly by low-angle normal faulting brings into question the importance of LANFs at early rift zones generally. LANFs are observed in continental rifts which, i) have undergone significant stretching and are close to breakup (e.g., Woodlark Rift, Taylor et al. 1999), ii) where there is significant magmatic activity or base-crustal shear stress to rotate stress tensors (e.g Basin and Range and central Apennines), or iii) have pre-existing thrust faults optimally orientated for reactivation (e.g., central Apennines). The Corinth Rift is an example of a mildly stretched rift, which is amagmatic and normal faulting is perpendicular to the Hellenide orogeny; thus none of these conditions apply. We suggest that although LANFs can become important in the transition to breakup, high-angle faulting will be the dominant strain accommodation mechanism in areas that have undergone limited stretching, do not have significant magmatic activity and do not have optimally orientated pre-existing low angle structures.

ACKNOWLEDGMENTS

We would like to thank Brian Taylor, Charles Williams and Rosa Polanco-Ferrer for insightful discussions. We thank the Computational Infrastructure for Geodynamics (geodynamics.org) which is funded by the National Science Foundation under award NSF-0949446. R. Gawthorpe would like to acknowledge Research Council of Norway PETROMAKS 2 Syn-rift Systems Project (255229/E30). Thanks to Mary Ford, Giovanni Camanni, an anonymous reviewer and Editor Dennis Brown for constructive comments.

REFERENCES CITED

Aagaard, B.T., Knepley, M.G., and Williams, C.A., 2013, A domain decomposition approach to implementing fault slip in finite-element models of quasi-static and dynamic crustal

deformation: Journal of Geophysical Research. Solid Earth, v. 118, p. 3059–3079, https://doi.org/10.1002/jgrb.50217.

Armijo, R., Meyer, B., King, G.C.P., Rigo, A., and Papanastassiou, D., 1996, Quaternary evolution of the Corinth Rift and its implications for the Late Cenozoic evolution of the Aegean: Geophysical Journal International, v. 126, p. 11–53, https://doi.org/10.1111/j.1365-246X.1996.tb05264.x.

Bell, R.E., McNeill, L.C., Bull, J.M., Henstock, T.J., Collier, R.E.L., and Leeder, M.R., 2009, Fault architecture, basin structure and evolution of the Gulf of Corinth Rift, central Greece: Basin Research, v. 21, p. 824–855, https://doi.org/10.1111/j.1365-2117.2009.00401.x.

Bell, R.E., McNeill, L.C., Henstock, T.J., and Bull, J.M., 2011, Comparing extension on multiple time and depth scales in the Corinth Rift, Central Greece: Geophysical Journal International, v. 186, p. 463–470, https://doi.org/10.1111/j.1365-246X.2011.05077.x.

Bernard, P., et al., 1997, The Ms = 6.2, June 15, 1995 Aigion earthquake (Greece): Evidence for low angle normal faulting in the Corinth rift: Journal of Seismology, v. 1, p. 131–150, https://doi.org/10.1023/A:1009795618839.

Collettini, C., De Paola, N., Holdsworth, R.E., and Barchi, M.R., 2006, The development and behaviour of low-angle normal faults during Cenozoic asymmetric extension in the Northern Apennines, Italy: Journal of Structural Geology, v. 28, p. 333–352, https://doi.org/10.1016/j.jsg.2005.10.003.

Elias, P., Kontoes C., Papoutsis I, Kotsis I., Marinou A., Paradissis D., Sakellariou D., 2009 Permanent Scatterer InSAR Analysis and Validation in the Gulf of Corinth: Sensors, v. 9. http://www.mdpi.com/1424-8220/9/1/46/htm

Ford, M., Rohais, S., Williams, E.A., Bourlange, S., Jousselin, D., Backert, N., and Malartre, F., 2013, Tectono-sedimentary evolution of the western Corinth rift (Central Greece): Basin Research, v. 25, p. 3–25, https://doi.org/10.1111/j.1365-2117.2012.00550.x.

Gessner, K., Ring, U., Johnson, C., Hetzel, R., Passchier, C.W., and Güngör, T., 2001, An active bivergent rolling-hinge detachment system: Central Menderes metamorphic core complex in western Turkey: Geology, v. 29, p. 611–614, https://doi.org/10.1130/0091-7613(2001)029<0611:AABRHD>2.0.CO;2.

Ghisetti, F., and Vezzani, L., 1999, Depth and modes of Pliocene–Pleistocene crustal extension of the Apennines (Italy): Terra Nova, v. 11, p. 67–72, https://doi.org/10.1046/j.1365-3121.1999.00227.x.

Jackson, J., Gagnepain, J., Houseman, G., King, G., Papadimitriou, P., Soufleris, C., and Virieux, J., 1982, Seismicity, normal faulting, and the geomorphological development of the Gulf of Corinth (Greece): The Corinth earthquakes of February and March 1981: Earth and Planetary Science Letters, v. 57, p. 377–397, https://doi.org/10.1016/0012-821X(82)90158-3.

Jolivet, L., Labrousse, L., Agard, P., Lacombe, O., Bailly, V., Lecomte, E., Mouthereau, F., and Mehl, C., 2010, Rifting and shallow-dipping detachments, clues from the Corinth Rift and the Aegean: Tectonophysics, v. 483, p. 287–304, https://doi.org/10.1016/j.tecto.2009.11.001.

King, T.A., 1998, Mechanisms of isostatic compensation in areas of lithospheric extension: Examples from the Aegean [Ph.D. Thesis]: Leeds, UK, University of Leeds.

Lambotte, S., Lyon-Caen, H., Bernard, P., Deschamps, A., Patau, G., Nercessian, A., Pacchiani, F., Bourouis, S., Drilleau, M., and Adamova, P., 2014, Reassessment of the rifting process in the Western Corinth Rift from relocated seismicity: Geophysical Journal International, v. 197, p. 1822–1844, https://doi.org/10.1093/gji/ggu096.

Lecomte, E., Le Pourhiet, L., and Lacombe, O., 2012, Mechanical basis for slip along low-angle normal faults: Geophysical Research Letters, v. 39, L03307, https://doi.org/10.1029/2011GL050756.

McNeill, L., Collier, R.L., De Martini, P., Pantosti, D., and D'Addezio, G., 2005, Recent history of the Eastern Eliki Fault, Gulf of Corinth: Geomorphology, palaeoseismology and impact on palaeoenvironments: Geophysical Journal International, v. 161, p. 154–166, https://doi.org/10.1111/j.1365-246X.2005.02559.x.

McNeill, L., Cotterill, C., Bull, J., Henstock, T., Bell, R., and Stefatos, A., 2007, Geometry and slip rate of the Aigion fault, a young normal fault system in the western Gulf of Corinth: Geology, v. 35, p. 355–358, https://doi.org/10.1130/G23281A.1.

Nixon, C.W., et al., 2016, Rapid spatiotemporal variations in rift structure during development of the Corinth Rift, central Greece: Tectonics, v. 35, p. 1225–1248, https://doi.org/10.1002/2015TC004026.

Palyvos, N., Lemeille, F., Sorel, D., Pantosti, D., and Pavlopoulos, K., 2008, Geomorphic and biological indicators of paleoseismicity and Holocene uplift rate at a coastal normal fault footwall (western Corinth Gulf, Greece): Geomorphology, v. 96, p. 16–38, https://doi.org/10.1016/j.geomorph.2007.07.010.

Parsons, T., and Thompson, G.A., 1993, Does magmatism influence low-angle normal faulting?: Geology, v. 21, p. 247–250, https://doi.org/10.1130/0091-7613(1993)021<0247:DMILAN>2.3.CO;2.

Resor, PG, 2008, Deformation associated with a continental normal fault system, western Grand Canyon, Arizona: Geological Society of America Bulletin. v. 120, p. 414-430

Rigo, A., Lyon-Caen, H., Armijo, R., Deschamps, A., Hatzfeld, D., Makropoulos, K., Papadimitriou, P., and Kassaras, I., 1996, A microseismic study in the western part of the Gulf of Corinth (Greece): Implications for large-scale normal faulting mechanisms:

Geophysical Journal International, v. 126, p. 663–688, https://doi.org/10.1111/j.1365-246X.1996.tb04697.x.

Sachpazi, M., Clément, C., Laigle, M., Hirn, A., and Roussos, N., 2003, Rift structure, evolution, and earthquakes in the Gulf of Corinth, from reflection seismic images: Earth and Planetary Science Letters, v. 216, p. 243–257, https://doi.org/10.1016/S0012-821X(03)00503-X.

Sachpazi, M., et al., 2007, Moho topography under central Greece and its compensation by Pn time-terms for the accurate location of hypocenters: The example of the Gulf of Corinth 1995 Aigion earthquake. Tectonophysics, 440 (1–4), 53–65. doi:10.1016/j.tecto.2007.01.009

Sibson, R.H., 1985, A note on fault reactivation: Journal of Structural Geology, v. 7, p. 751–754, https://doi.org/10.1016/0191-8141(85)90150-6.

Sorel, D., 2000, A Pleistocene and still-active detachment fault and the origin of the Corinth-Patras rift, Greece: Geology, v. 28, p. 83–86, https://doi.org/10.1130/0091-7613(2000)28<83:APASDF>2.0.CO;2.

Taylor, B., Goodliffe, A. M., and Martinez, F., 1999, How continents break up: insights from Papua New Guinea: Journal of Geophysical Research: Solid Earth (1978-2012), v. 104, no. B4, p. 7497-7512.

Taylor, B., Weiss, J.R., Goodliffe, A.M., Sachpazi, M., Laigle, M., and Hirn, A., 2011, The structures, stratigraphy and evolution of the Gulf of Corinth rift, Greece: Geophysical Journal International, v. 185, p. 1189–1219, https://doi.org/10.1111/j.1365-246X.2011.05014.x.

FIGURE CAPTIONS

Figure 1. A: Corinth Rift bathymetry and major active and inactive faults. Red box shows the location of microseismicity data in B. Yellow line shows location of seismic profile in Fig. DR1. Pink dashed line shows location of the profile in B. B: Composite cross-section across the western Corinth Rift to show proposed deep fault geometry models. Dark grey represents syn-rift fill offshore, onshore syn-rift is not represented. Microseismicity from Lambotte et al. (2014): Blue dots are micoseismicity between 2000 and 2007, red dots 1995, green dots 1991. Note, microseismicity data has been projected onto this profile from further west. Focal mechanism for July 1995 earthquake (Bernard et al. 1997).

Figure 2. Finite-element model setup. Open circles indicate free-slip boundaries.

Figure 3. Effect of changing fault geometry on the coseismic and long-term displacement field, per meter of slip on a normal fault in 40 km thick layered viscoelastic crust. The graph shows the displacement of the Earth's surface and the colored models show vertical displacements in 2-D for coseismic slip and after 30 k.y. of post-seismic relaxation. A: Model 1a: Fault dipping at 45° from the surface to 7 km depth, then 15° to 10 km (brittle-ductile transition). B: Model 1b: Fault dipping at 45° from the surface to 3 km depth, then 20° down to 10 km. C: Model 2a: planar fault dipping at 45° from the surface down to 10 km. d) Model 2b: planar fault dipping at 45° from the surface down to 10 km.

Figure 1

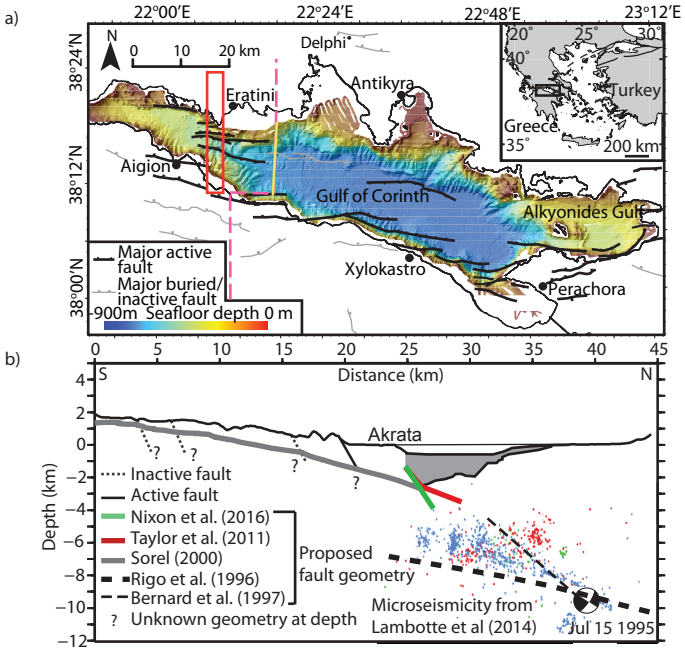
a)
22°00′E
22°24′E
22°48′E
23°12′E
38°24′N
38°12′N
38°00′N
N
0 10 20 km
Delphi
Antikyra
Eratini
Aigion
Gulf of Corinth
Alkyonides Gulf
Xylokastro
Perachora
Major active fault
Major buried/ inactive fault
900m Seafloor depth 0 m
20°
25°
30°
40°
35°
Turkey
Greece
200 km
b)
0 5 10 15 20 25 30 35 40 45
Distance (km)
S
N
Akrata
Depth (km)
4 2 0 −2 −4 −6 −8 −10 −12
Inactive fault
Active fault
Nixon et al. (2016)
Taylor et al. (2011)
Sorel (2000)
Rigo et al. (1996)
Bernard et al. (1997)
? Unknown geometry at depth
Proposed fault geometry
Microseismicity from Lambotte et al (2014)
Jul 15 1995

Figure 2

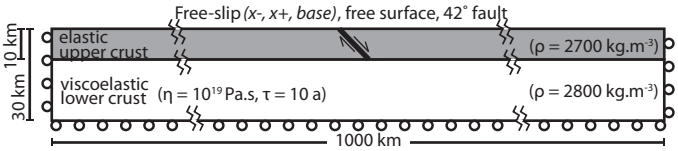
Free-slip (x-, x+, base), free surface, 42° fault
10 km
elastic
upper crust
(ρ = 2700 kg.m-3)
30 km
viscoelastic
lower crust
(η = 10^19 Pa.s, τ = 10 a)
(ρ = 2800 kg.m-3)
1000 km

Figure 3

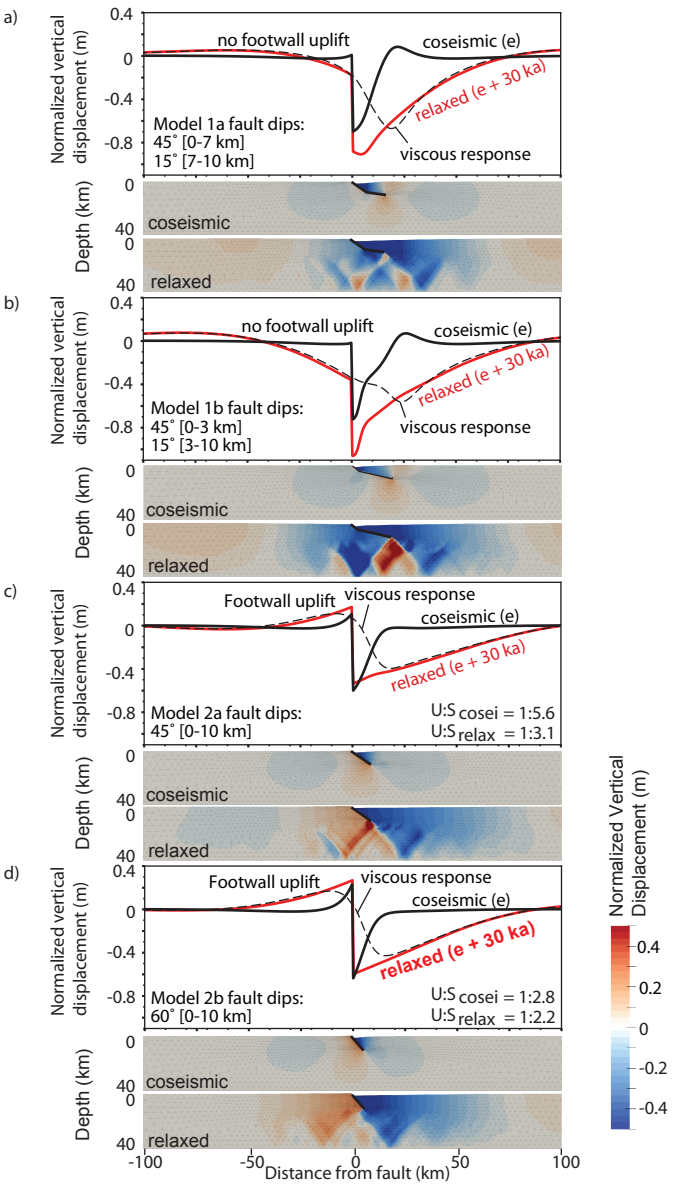
a)
b)
c)
d)
Normalized vertical displacement (m)
Depth (km)
no footwall uplift
coseismic (e)
relaxed (e + 30 ka)
viscous response
Model 1a fault dips:
45° [0-7 km]
15° [7-10 km]
Model 1b fault dips:
45° [0-3 km]
15° [3-10 km]
Footwall uplift
Model 2a fault dips:
45° [0-10 km]
U:S cosei = 1:5.6
U:S relax = 1:3.1
Model 2b fault dips:
60° [0-10 km]
U:S cosei = 1:2.8
U:S relax = 1:2.2
coseismic
relaxed
Distance from fault (km)
Normalized Vertical Displacement (m)